

Laboratory Measurements of Sea Ice: Connections to Microwave Remote Sensing

Ronald Kwok, *Member, IEEE*, Son V. Nghiem, *Member, IEEE*, S. Martin, D. P. Winebrenner, *Senior Member, IEEE*, Anthony J. Gow, Donald K. Perovich, C. T. Swift, *Fellow, IEEE*, David G. Barber, K. M. Golden, and E. J. Knapp

Abstract—The connections between laboratory measurements and remote-sensing observations of sea ice are explored. The focus of this paper is on thin ice, which is more easily simulated in a laboratory environment. We summarize results of C-band scatterometer measurements and discuss how they may help in the interpretation of remote-sensing data. We compare the measurements with observations of thin ice from ERS and airborne radar data sets. We suggest that laboratory backscatter signatures should serve as bounds on the interpretation of remote-sensing data. We examine these bounds from the perspective of thin ice signatures, the effect of temperature, and surface processes, such as frost flowers and slush on these signatures. Controlled experiments also suggest new directions in remote-sensing measurements. The potential of polarimetric radar measurements in the retrieval of thickness of thin ice is discussed. In addition to the radar results, we discuss the importance of low-frequency passive measurements with respect to the thickness of thin ice.

I. INTRODUCTION

EVEN though thin ice occupies a small areal fraction of the Arctic sea ice cover, the flux of heat from the relatively warm ocean through this ice is comparable to that

integrated over the larger fraction of thicker ice [16]. Hence, the identification of thin ice in remote-sensing data has been an important goal for providing measurements to support a variety of process studies and climate change research. Active and passive microwave sensors are the current sensors of choice because of their day and night viewing capabilities and because they are relatively unaffected by clouds and other atmospheric conditions. An additional quality of active microwave sensors, like scatterometers and synthetic aperture radars (SAR's), is that they provide high-resolution mapping of the polar ice covers. However, the goal of deriving ice thickness from microwave data sets has proved elusive because these sensors do not provide direct measurements of ice thickness. The emissivity and backscatter are measurements of the surface and volume electromagnetic properties of sea ice, which are only sometimes correlated to ice thickness. Rather than classify the microwave observations into specific thickness categories, current routine analyses [3], [12] of these data sets provide coarse ice types (e.g., multiyear ice, first-year ice, etc.) as proxy indicators of ice thickness. The interpretation and resolution of the thin ice category are typically rather poor due to the variability in the active and passive signatures of thin ice.

In this paper, we focus on the interpretation of thin ice signatures in microwave data in the context of laboratory scatterometer measurements. Generally, the interpretation of sea ice remote-sensing data have been guided by field experiments and laboratory measurements. Field measurements have provided observations that characterize, to a limited extent, the natural variability of sea ice. Laboratory measurements are unique because the evolution of the signature of sea ice can be observed in a controlled environment and provide us with a different perspective with respect to remote sensing. It is this connection, between laboratory measurements and remote sensing, which we would like to explore here. We have observed the growth of sea ice, with the Jet Propulsion Laboratory (JPL)¹ C-band polarimetric scatterometer, under different conditions using the sea ice facilities at the United States Army Cold Regions Research and Engineering Laboratory (CRREL), Hanover, NH. These experiments were conducted over a period of three years from 1993 to 1995. One of the objectives was to understand the relationship between the morphological and physical characteristics and the observed electromagnetic properties of sea ice. These relations are easier

Manuscript received October 31, 1997; revised June 22, 1998. The work of R. Kwok and S. V. Nghiem was carried out at the Jet Propulsion Laboratory, California Institute of Technology, and was supported by the National Aeronautics and Space Administration (NASA) and the Office of Naval Research (ONR) through an agreement with NASA. The work of S. Martin was supported by ONR Contract N00014-90-J-0161. The work of D. P. Winebrenner was supported by ONR Grants N00014-89-J-3132 and N00014-96-1-0266 and by NASA Grant NAGW-1256. The work of A. J. Gow and D. K. Perovich was supported by ONR Contracts N00014-95-MP-3002 and N00014-95-MP-3019. The work of C. T. Swift and E. J. Knapp was supported by ONR. The work of K. M. Golden was supported by ONR Grants N00014-93-10 141 and N00014-94-10 958. The work of D. G. Barber was supported by the Polar Continental Shelf Project by ONR Grant N00014-94-1-03-86 and the Natural Sciences and Engineering Research Council (NSERC).

R. Kwok and S. V. Nghiem are with the Jet Propulsion Laboratory, California Institute of Technology, Pasadena, CA 91109 USA (e-mail: ron@rgps1.jpl.nasa.gov; nghiem@solar.jpl.nasa.gov).

S. Martin is with the School of Oceanography, University of Washington, Seattle, WA 98195 USA.

D. P. Winebrenner is with the Applied Physics Laboratory, University of Washington, Seattle, WA 98105 USA.

A. J. Gow and D. K. Perovich are with the Snow and Ice Branch, U.S. Army Cold Regions Research and Engineering Laboratory, Hanover, NH 03755 USA.

C. T. Swift and E. J. Knapp are with the Microwave Remote Sensing Laboratory, University of Massachusetts, Amherst, MA 01003 USA.

D. G. Barber is with the Department of Geography, University of Manitoba, Winnipeg, Man., R3T 2N2 Canada.

K. M. Golden is with the Department of Mathematics, University of Utah, Salt Lake City, UT 84112 USA.

Publisher Item Identifier S 0196-2892(98)06691-1.

¹JPL is part of the California Institute of Technology, Pasadena.

to establish in a controlled environment, but the utility of such links have not been fully explored from the remote-sensing point of view. One obvious difference is the scale of the observations between laboratory measurements and remote-sensing data sets. In this paper, we address the role of the laboratory measurements in the interpretation of thin ice with remote-sensing data. Presently, several spaceborne SAR's including ERS-1, ERS-2, and RADARSAT, all of which are operated at C-band, are providing routine observations of the polar regions. In particular, the recently launched RADARSAT is providing better than weekly coverage of the Arctic Ocean. If algorithms could be devised to provide more definitive and quantitative results on thin ice, it would be a significant contribution to the understanding of processes of the polar regions.

In the following sections, we describe several laboratory experiments and their relevance to remote sensing. These experiments were designed to investigate the effects of surface and volume processes on the backscatter signature of thin ice. The processes include the growth of frost flowers, the effect of a wet slush layer, and the responses of sea ice due to diurnal cycles of insolation and air temperature. The paper is organized as follows. In the next section, we discuss the possible role of laboratory measurements. Section III describes our instrumentation and the experiments we have conducted at CRREL. In Section IV, we compare our laboratory measurements with the observations of thin ice from airborne and spaceborne radars and discuss whether the laboratory measurements could constrain our interpretation of remote-sensing data. Section V presents the potential of polarimetric radar observations for the retrieval of thin ice thickness. We also discuss passive measurements with low-frequency radiometers with respect to the thickness of thin ice. The last section summarizes the paper.

II. ROLE OF LABORATORY MEASUREMENTS

The role of laboratory measurements in the observation of thin ice is discussed. We focus our attention on C-band signatures since the current spaceborne SAR, which are providing routine observations of the polar regions, are operated at this frequency. This ice type is most easily grown in a controlled environment due to its high growth rate. The similarity of the structural and physical properties of laboratory grown sea ice and sea ice in its natural environment was discussed in [22].

We recognize that thin ice exists in a variety of forms in its natural environment and that it is neither practical nor desirable to simulate all its expressions in the laboratory. As we alluded to above, there is a large-scale difference between the resolution of a spaceborne SAR sensor (tens of meters) and a laboratory scatterometer (meters). Within a SAR resolution element, there are areal mixtures of various forms of thin and thick ice, whereas a laboratory scatterometer typically provides measurements of a pure type. Some of the surface processes (e.g., frost flowers, slush formation, etc.) that dominate the backscatter properties of thin ice could be readily reproduced; other ice types (e.g., rafted ice, composite pancake ice, etc.) that are created by

mechanical processes over extended scales are less readily fabricated. Because of differences in sensor resolutions and variabilities in sea ice types, laboratory measurements should not be applied directly to the interpretation of remote-sensing observations. In this regard, the role of laboratory measurements should be to establish the bounds and limits in the retrieval of sea ice parameters in remote-sensing data sets.

Laboratory experiments also allow continuous monitoring of ice growth as well as the surface processes associated with that growth. This is in contrast to the sparse sampling obtained from spaceborne sensors. For example, continuous changes in thin ice signature (discussed later) due to diurnal cycles of insolation and air temperature are difficult to resolve with spaceborne sensors. In the laboratory, the mechanisms that contribute to such backscatter variability can be examined directly and correlated with their *in-situ* temperature and salinity profiles together with ice properties from ice cores. Understanding the physical processes that contribute to radar observables are important in the development of a retrieval algorithm for sea ice properties using satellite radar data.

With the polarization capability of our scatterometer, laboratory ice measurements provide a full set of polarimetric backscattering coefficients. In the experiments, polarimetric calibration instrumentation is setup accurately and calibration data are taken frequently. In view of polarization differences between ERS and RADARSAT, understanding of the polarimetric responses of sea ice are important. To fully utilize colocated data from these sensors, the polarization differences need to be considered. Also, future spaceborne SAR's like LIGHTSAR and ESA's ENVISAT will likely provide multipolarization observations, and laboratory polarimetric measurements could provide indications of the potential of these measurements.

III. LABORATORY EXPERIMENTS

A. CRREL Indoor and Outdoor Facilities

We conducted our experiments at the indoor and outdoor facilities at CRREL. The indoor facility is a room that measures about 6×7 m on the floor and approximately two stories high with the refrigeration units mounted on the ceiling. The refrigeration system is capable of taking the air temperature to below -28 °C and controlling it to within 2 °C. The freezing pool, approximately 1.2 m in depth, occupies most of the area. We line the walls of the room with radar anechoic material to reduce unwanted reflections and multipath contamination of the returns from the sea ice. The radar is mounted about 3 m above the ice such that the surface is in the antenna far-field.

The outdoor facility, named the CRREL Geophysical Research Facility (GRF), is a pool of approximately 18×7.5 m in dimension with a depth of 2 m. A structure with an insulated roof, which slides on rails, can be moved over the ice sheet to shield the ice from the elements, such as sun, snow, and rain. Cooling units are attached to this structure at one end of the pool. The refrigeration system can cool the air temperature

to -18°C over the ice sheet when the structure covers the growing ice. At the other end of the pool is a 4-m-high gantry, where the scatterometer was mounted during the experiments. The height of the radar above the ice sheet was approximately 4 m. The gantry was designed to move along the rails to different parts of the pool for obtaining measurements of different areas of the ice sheet. The control and measurement instrumentation were set up in a tent located on one corner of the GRF.

We successfully fabricated a variety of saline ice sheets during the CRREL experiments (CRRELEX). Those ranged from thin new ice simulants to thermally modified ice sheets whose physical and structural properties closely mimicked Arctic second-year ice. Depending on the nature of the experiment, both under-the-roof refrigeration and natural freezing under open-air conditions were utilized in the fabrication of CRRELEX ice sheets. Ice grown indoor and during roof-on at the GRF simulates, in process and properties, those formed under dark winter conditions (no insolation) in the Arctic.

B. Ice Growth and Physical Characteristics

Nature of the Freezing Process: Once a continuous ice sheet has formed, the underlying water is isolated from the cold air, allowing latent heat to be extracted through the ice sheet by thermal conduction. Direct freezing of salt water to the underside of the ice is called congelation growth, typically yielding vertically elongated columnar crystals. These crystals are characterized by a vertical substructure consisting of ice plates interspersed with parallel layers of brine inclusions. Such a substructure results from the dendritic nature of the freezing interface, occurring in response to the buildup of brine at the interface. Excess brine that cannot be expelled from the interface is systematically incorporated into the spaces between the dendrites. Actual incorporation of brine into the ice structure occurs by pinching off of the interdendrite spaces, leading to the formation of individual pockets of brine and creation of the characteristic ice plate and brine layer substructure of the saline ice crystals. The overall process of the freezing of seawater in the polar oceans is described in greater detail by [7] and [32]. An essentially identical process was duplicated in the freezing of saline ice sheets at CRREL. The growth process and structural and physical properties of the laboratory ice are shown to be similar to Arctic sea ice [22].

Temperature and Salinity Effects: Changes with time in the overall structure of sea ice occur mainly in response to temperature changes in the ice. Brine inclusions are particularly sensitive in this regard. In the event of protracted warming, brine pockets expand and their subsequent coalescence generally leads to channelization and downward drainage of the brine, with resultant desalination of the ice. The incorporation of brine into sea ice is the most important parameter effecting the mechanical, thermal, and electromagnetic properties of the ice. In the case of the electromagnetic properties of the ice, it is the concentration and distribution of brine in the ice that largely determines the nature of the scattering signature and its interpretation. Many of the salinity profile characteristics

exhibited by saline ice sheets fabricated during CRRELEX duplicated those of Arctic sea ice, including the following:

- 1) high salinities at the top and bottom of thinner ice sheets, leading to the formation of the c-shaped profile;
- 2) general weakening of the c-shaped profile with increasing thickness and age of the ice;
- 3) substantial desalination of the upper levels of older ice subjected to protracted warming or surface melting.

Characterization of Physical Properties: An ice characterization study conducted in support of the remote-sensing program at CRREL includes monitoring of ice thickness changes as influenced by such factors as surface air temperature, wind chill, and radiation fluxes. Vertical profile measurements of water and ice temperatures, salinity, and density and their derived properties, brine volume and entrapped air content (porosity), are also performed. Thin sections cut from samples from the growing ice sheet are used to investigate crystalline structure and brine inclusion relationships essential to assessing both the qualitative and quantitative aspects of salt entrapment. This work was supplemented by image processing of thin section photographs to statistically describe volume-scattering characteristics via correlation functions and inclusion size distribution statistics of the various ice types [27]. C-shaped profiles, typical of young sea ice growth in the Arctic, characterize the earlier stages of growth of the laboratory ice. Later profiles reflect the desalinating effects of elevated air temperature occurring during the latter stages of saline ice growth. The elongated nature of the crystals and the ice plate/brine inclusion substructures precisely duplicate the same features observed in young sea ice in the Arctic.

Sea Ice Permittivities: Permittivities of sea ice govern electromagnetic wave propagation, attenuation, and scattering. Thus, the permittivities are a determining factor of the microwave remote-sensing observables. It is useful to characterize the bulk electromagnetic behavior through an effective complex permittivity ϵ_{eff} that incorporates scattering effects. The geometry and relative volume fraction of the brine inclusions depend strongly on ice growth conditions, such as ice temperature and salinity distribution in the ice layer. A comprehensive series of rigorous bounds on ϵ_{eff} valid in the quasistatic regime has been developed [5], [6], [30]. Given an increasing amount of information on the sea ice microstructure, such as the brine volume fraction or further assuming statistical isotropy within the horizontal plane, the bounds restrict ϵ_{eff} to an increasingly small region of the complex ϵ_{eff} -plane. A different approach based on strong fluctuation theory, accounting for sea ice thermodynamic cycling, has been developed [21] to obtain complex anisotropic effective permittivity tensor $\bar{\epsilon}_{\text{eff}}$, valid not only in the quasistatic regime, but for higher frequencies as well.

C. JPL C-Band Polarimetric Scatterometer

The polarimetric scatterometer operates at C-band with a center frequency of 5 GHz and a bandwidth of 1 GHz. Stepped frequencies are synthesized by a network analyzer and coupled to free space through a diagonal horn antenna. The antenna is dual-polarized with a beamwidth of 12° and a gain of 22.6 dBi

at the center frequency. Raw data are compressed and recorded in a computer that also controls the polarization switching and the network analyzer.

To prevent drift in the radio-frequency (RF) subsystem, the electronics are maintained at room temperature (25 °C) with a temperature controlling unit. The antenna is steered in azimuth and elevation using two independent motors attached to an assembly containing the antenna and RF subsystem. Calibration targets include corner reflectors, spheres, and external backgrounds. Calibration measurements are made periodically during the experiments. We estimate the overall uncertainty in the radar measurements to be approximately 1.2 dB. The recorded data were calibrated and processed into a polarimetric covariance matrix format after the experiments. The noise-equivalent σ_0 of the radar is at -45 dB for copolarized measurements and -55 dB for cross-polarized measurements. The low noise floor is achieved with a coherent-subtraction technique and a system design that avoids internal signal reflections. A more detailed description of the scatterometer can be found in [22].

The polarimetric scatterometer measures the four elements of the scattering matrix $\bar{\bar{S}}$, where

$$\bar{\bar{S}} = \begin{bmatrix} f_{hh} & f_{hv} \\ f_{vh} & f_{vv} \end{bmatrix}.$$

The conventional backscattering coefficients $\sigma_{hh}, \sigma_{hv}, \sigma_{vh}, \sigma_{vv}$ and the copolarized polarimetric scattering coefficient σ_{hhvv} are determined by $\langle f_{hh}f_{hh}^* \rangle, \langle f_{hv}f_{hv}^* \rangle, \langle f_{vh}f_{vh}^* \rangle, \langle f_{vv}f_{vv}^* \rangle$, and $\langle f_{hh}f_{vv}^* \rangle$, respectively. The angular brackets represent the ensemble average, and the asterisk denotes the complex conjugate. Two other frequently used parameters (normalized) that are derived from these coefficients are

$$\rho = \frac{\sigma_{hhvv}}{\sqrt{\sigma_{hh}\sigma_{vv}}}$$

which is the complex correlation coefficient between the hh and vv channels; the copolarized phase can be computed directed from this complex quantity. And the ratio of the magnitude of the copolarized returns is

$$\gamma = \frac{\sigma_{vv}}{\sigma_{hh}}.$$

D. The Experiments

These experiments were designed to investigate the relationship between the scatterometer observations and the various physical surface conditions and volume characteristics of thin ice and support the validation sea ice scattering models. Here, we summarize the experiments starting with the simple constant ice growth, then we present a more complex growth of frost flowers on ice surface, the flooding and slush layer on sea ice, and the effects of diurnal thermal cycling.

Thin Ice Signature: The thin ice was grown under quiescent conditions without wind or wave action in the indoor facility, where the temperature was well controlled. Saline ice was grown under constant air and water temperatures, representing the simplest ice growth conditions. The experiments were repeated at slightly different air temperatures. In all cases,

the mean air temperatures were kept below -20 °C. The indoor air temperatures fluctuated slightly around the mean and an rms deviation of $\pm 0.1^\circ$ was maintained. Measurements of thickness and growth rate, temperatures and salinities, crystallographic structures, brine layer, and cellular substructure spacing show that laboratory grown ice has characteristics very similar compared to those of thin sea ice in Arctic leads [22]. The results from these experiments serve as a baseline for comparison with subsequent experiments that study the effects of surface and volume processes on thin ice signature. In all our measurements, the thickness of the ice reached 12 cm in several days of ice growth. All scatterometer measurements were made at the incidence angle range from 20 to 40°.

Effect of Frost Flowers: In two of our experiments, the temperature in the indoor facility was maintained below -28 °C. We found that low temperature was conducive to the growth of frost flowers. Polarimetric radar data were taken during the flower growth together with a time series of still photography, video recording, and physical characteristics of frost flowers. Further details of the experiment were described by [23]. The frost flowers consist of 10–30-mm-high fragile saline ice crystals that grow on the ice surface and are accompanied by the formation of a 1–4-mm-thick slush layer under the flowers. We characterize this surface process in terms of the spreading rate of the flowers and slush layer, the height of the flowers and its salinity, the thickness and salinity of the slush layer, and the salinity of the adjacent bare ice. Frost flowers close to 90% areal coverage of the ice surface was achieved. Polarimetric measurements were collected at frequent intervals throughout the experiment. Measurements were made with the full frost flower structure, with the flower ice crystals removed, and with the slush layer removed to assess the contribution of these components to the total scattering cross section of thin ice. These experiments studied only the growth stage of frost flower; the temporal evolution of the decay stage and surface modifications with its associated backscatter response were not investigated.

Effect of Flooding and Slush Formation: We investigated the effect of flooding and the formation of slush layer on the signature of thin ice in one experiment. Saline water was taken from beneath the ice sheet and flushed onto the ice surface. On the cold ice surface, the water on the surface started to freeze immediately, forming a wet slushy layer. Polarimetric measurements were obtained for normal and oblique incidence angles. For normal incidence, the reflectivity is strongly modified because of the high permittivity of the slush layer. Backscatter at oblique angles is also changed significantly by the slush layer. The thickness of the slush layer was measured immediately before scatterometer data acquisition. Samples of the slush layer and the ice layer were taken for ice characteristics measurements.

Effect of Diurnal Cycling: We conducted this experiment at the outdoor GRF facility to study the effects of diurnal temperature cycles on polarimetric scattering signatures of sea ice [24]. The roof of the GRF was removed to take advantage of the natural diurnal warming and cooling. An ice sheet was grown from open water over a period of 2.5 days. This duration allowed us to investigate the repeatability of the radar

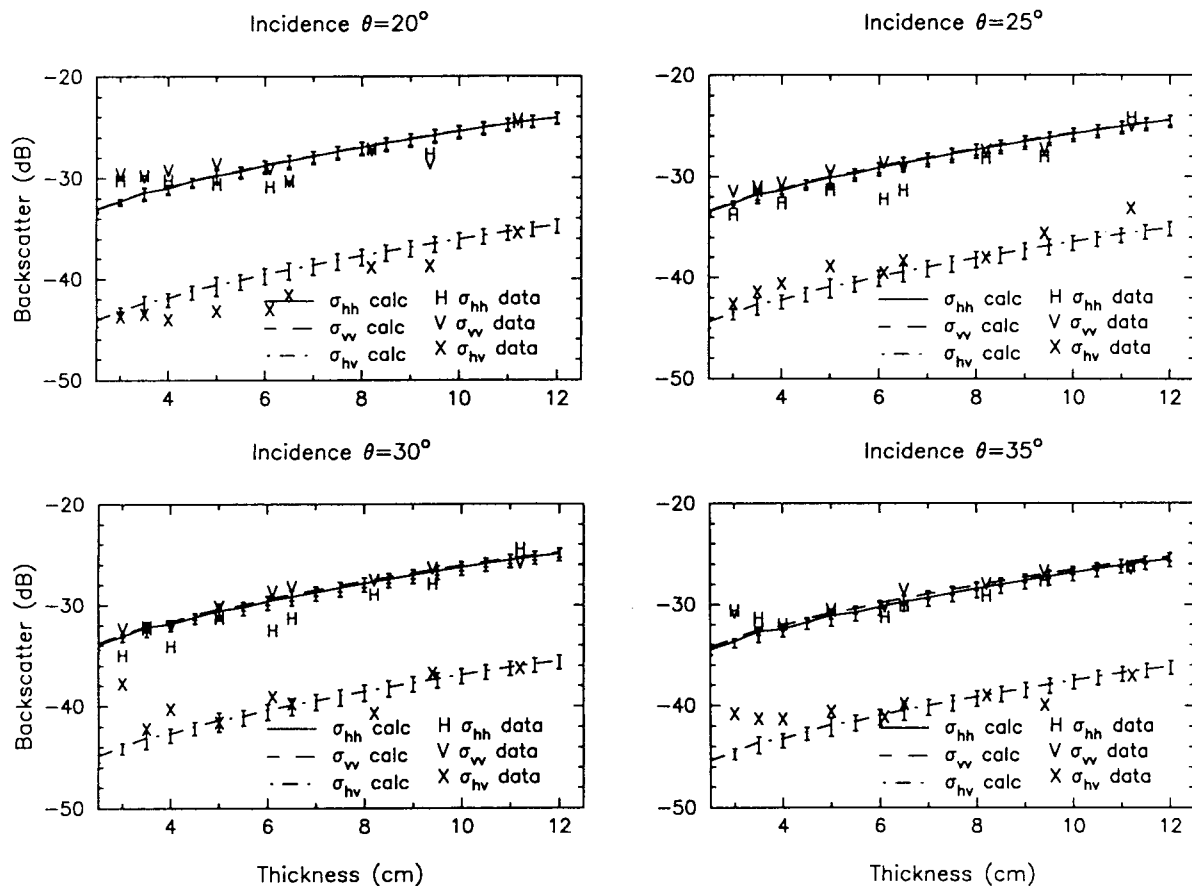


Fig. 1. C-band backscatter of thin ice grown under laboratory conditions. Capital letters represent measured data, and curves are model calculations [22] with a Gaussian thickness distribution with mean thickness from 2.5 to 12 cm.

signatures and determine whether the diurnal thermal effects are reversible. During the experiment, the air temperature varied between -12°C during day to -36°C at night. The initial growth rate was slow during the day due to the insolation under clear sky conditions. Throughout the night, the growth rate increased significantly as the temperature dropped. Polarimetric scatterometer measurements were carried out over two temperature cycles for the duration of the experiment. Calibration measurements were also made throughout the experiment to monitor the scatterometer system stability. Data, including air temperatures, ice temperature profiles, ice salinity profiles, and ice thicknesses, were taken periodically.

IV. RELEVANCE TO REMOTE SENSING

A. Thin Ice (0–12 cm) Backscatter

Thin ice backscatter signature at C-band over the ERS SAR spans a range of look angles ($19\text{--}26^\circ$), and VV-polarization spans a range from approximately -30 dB to as high as -5 dB. The lower bound in the backscatter can be established by our scatterometer measurements in the laboratory. Field programs [4], [19] typically observe backscatter that are higher than what is obtained in the laboratory quiescent ice growth. The thin ice (dark nilas) grown in the quiescent conditions in the laboratory has very smooth surfaces. Any perturbation to that smooth surface introduces an additional component to the total radar

cross section, resulting from the superimposed roughness. Thus, the unperturbed laboratory measurements provide a reasonable lower bound. The upper bound is established (disregarding any mechanical deformation of the thin ice) probably by frost-flower-covered thin ice. We discuss in more detail the phenomenon of frost flowers in the next subsection.

If the scatterometer measurements establish the lower bounds of backscatter for a range of ice thicknesses, what can we say about the backscatter signature observed in spaceborne SAR's, such as ERS-1? Fig. 1 shows a plot of the dependence of backscatter on thickness of laboratory grown thin ice. It is clear that the level of backscatter of ice at these thicknesses are below the noise floor of the ERS radars (approximately -24 dB) and therefore not resolved by the sensor if thin ice similar to that of laboratory ice were observed. We could, however, say that if an observed pixel is at or close to the noise floor of the ERS-1 sensor, there is a high likelihood that the pixel contains thin ice of thickness less than, say, 10 cm (see Fig. 1). This is because thicker ice types generally have higher backscatter than thin ice in this thickness range [10]. Of course, thin ice could have a higher backscatter due to mechanical deformation, which we cannot address with the laboratory measurements.

We show in Fig. 2 two ERS-1 images of the same geographic area separated by three days. This image pair of the ice cover shows large openings that were created during

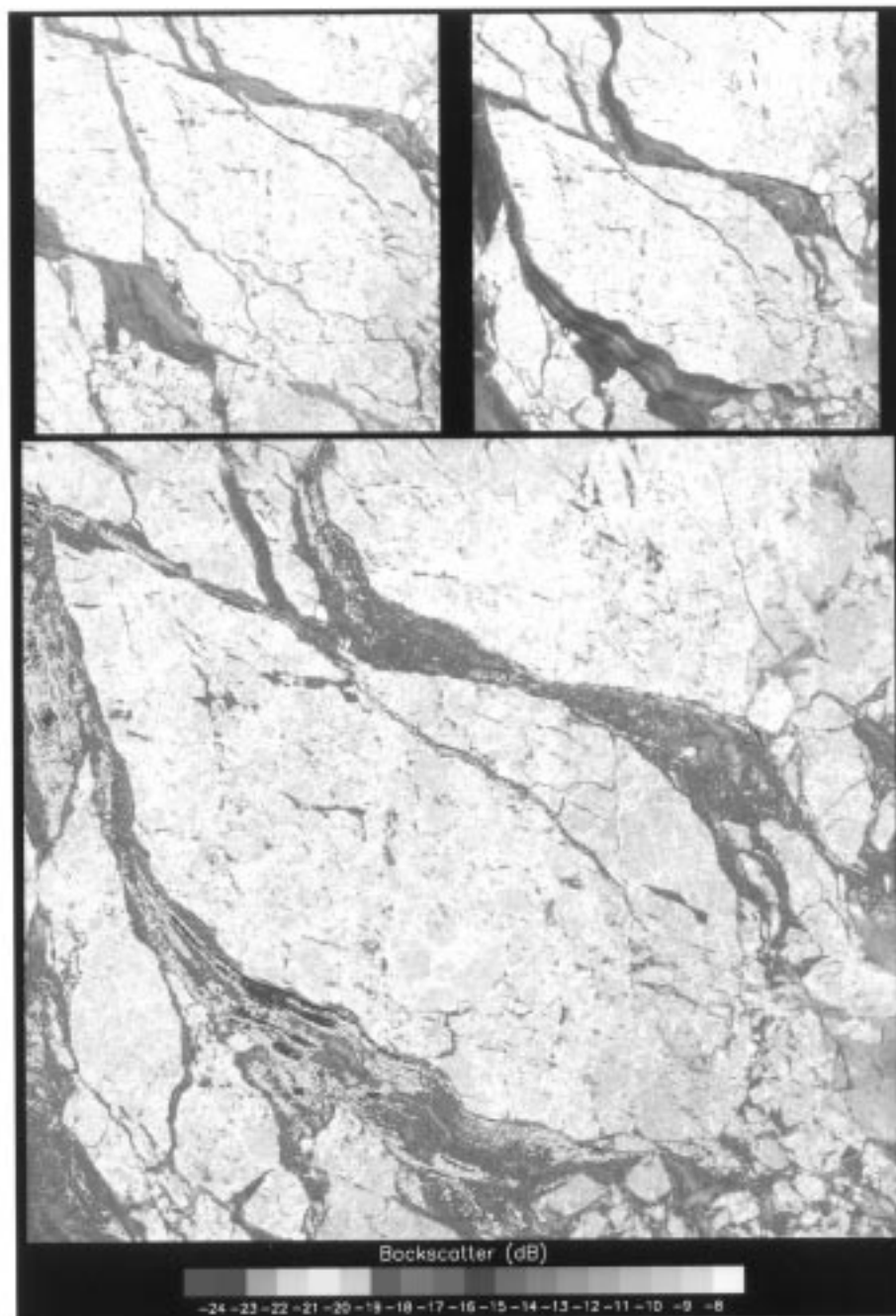


Fig. 2. Upper panels are a pair of ERS-1 images showing large openings created during the observed time interval of three days. Lower panel shows backscatter of young sea ice in the opening.

the interval between the repeat observations. The ice in this opening must be between zero and three days old, which is determined strictly from ice motion [9]. The structure of the features suggests that the openings were not created by a single event, but rather several openings and maybe closings over the three days. If the ice were three days old and the ambient temperature was around -20°C , the thickness of the ice is most likely less than 20 cm thick, estimated with a simple freezing-degree day calculation [17]. Sea ice with a range of backscatter (between -24 and -19 dB) can be seen in the

leads. The brightest backscatter is probably from frost flowers in the leads. To explore the signature evolution further, we follow the backscatter history of these openings as the ice thickens with time. The time sequence presented in Fig. 3, which spans a period of nine days, shows that the backscatter increases over time. Note that the uncertainty of the calibration is approximately 1–2 dB. This particular example demonstrates that the lower bound discussed above is reasonable for thin ice. For remote sensors with higher signal-to-noise ratio (SNR) or lower noise-equivalent σ_0 , such as an airborne SAR, the lower

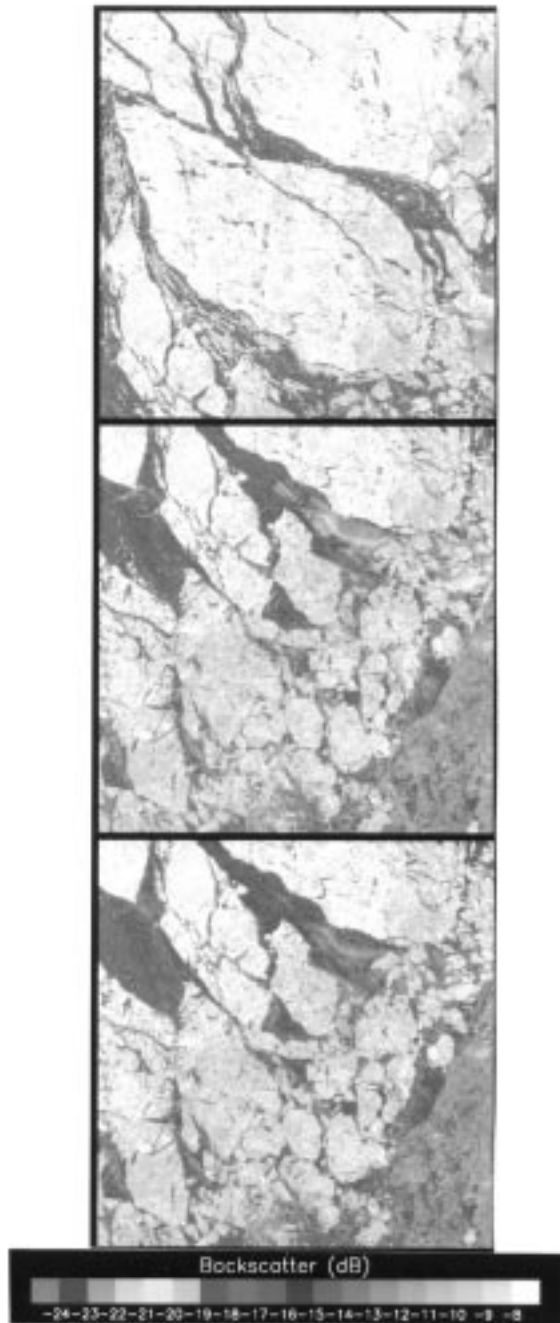


Fig. 3. Time-series of ERS-1 images in the Arctic showing the evolution of sea ice backscatter in openings as the ice thickens with time.

backscatter can indeed be observed. For example, if the noise-equivalent $\sigma_0 = -30$ dB, the lower limit corresponds to ice thinner than 5 cm (Fig. 1).

B. Frost Flowers on Thin Ice

On the other extreme of radar return is the enhancement of the backscatter of thin ice due to the growth of frost flower on the surface. This high backscatter from thin young ice has been attributed to the formation of frost flowers [25], [31]. A description of the physical characteristics of the frost flowers can be found in [13] and more recently in [15] and

[26]. The best illustration of the evolution of the signature of thin ice with frost flower is with the sequence of five ERS-1 images, which spans a 12-day period (Fig. 4). The initial increase in backscatter during the first several days of ice growth immediately after the opening of the lead and the slow decay of the signature to that of thicker first-year ice are characteristic of this surface process. We have observed in ERS-1 SAR (C-VV) imagery a large number of new leads containing sea ice with high initial backscatter and with similar backscatter history. We have also observed cases in which the backscatter of sea ice in leads that remained relatively low for an extended period of time (days) and slowly attaining the higher backscatter of thicker first-year ice. We cannot say, without a more extensive and systematic study, which path of backscatter evolution is more typical. It is dependent on local meteorological conditions; however, the detailed *in situ* measurements to support such investigations are typically not available.

We list three motivations for studying this phenomenon. First, field observations in the Beaufort [26] suggest that frost flowers appear with some frequency during the Arctic cold season. Second, the surface modification by the frost flowers alter the thermal and surface properties of young sea ice. Third, the mechanism that causes an enhancement in the backscatter (more than 200% increase) over that of flower-free young ice. From the remote-sensing perspective, the significance of flower growth and the associated changes in the surface salinity to radar observations is that understanding these processes is a step toward explaining the large variability in the signature of newly formed ice and better interpretation of radar remote-sensing data. If indeed there is large modification to the thermal properties of new ice, this effect is significant in heat flux calculations over this ice type.

The growth of frost flowers in the laboratory was first reported by [14]. Our C-band laboratory measurement of the scattering signature was discussed in detail by [23]. The laboratory experiments provided observations of the initial evolution of the signature and not the decay due to the length of the process. Fig. 5 shows a time series of the frost flower coverage of the ice surface during our experiment until a 90% areal coverage was achieved. Fig. 6 illustrates the effect on flower covered thin ice. The measurements indicate that it is the slush layer below the low-density ice crystals (Fig. 6) that contributes most to the enhancement in the backscatter. After the removal of this high-saline slush layer, the backscatter level returns to that of thin ice (discussed above). The laboratory measurements are lower than that observed in remote-sensing data, probably due to the density and height of frost flowers grown in our environment and differences in ice thickness and surface roughness. Nevertheless, these results showing 3–5-dB backscatter increase due to frost flowers are consistent with the backscatter increase (up to 6 dB) in ERS-1 data in Fig. 6. The experiment suggests that a transient increase of 5 dB in thin ice backscatter can be used as an indicator for a full coverage (~90%) in the growth stage of frost flowers.

From the perspective of remote sensing, frost flowers are difficult to identify unambiguously in single SAR images due to the range of backscatter level and its time-dependent be-

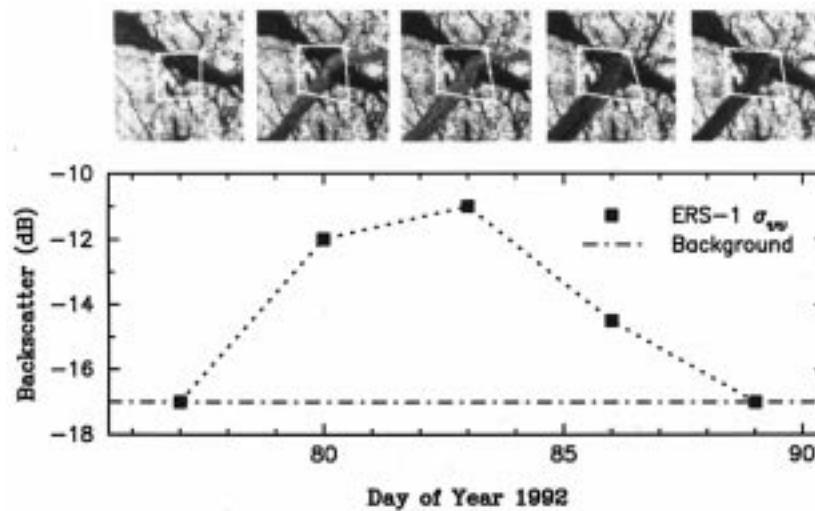


Fig. 4. Sequence of ERS-1 images over a 12-day period, illustrating the growth and decay of frost flowers in an Arctic leads with the corresponding transient response in backscatter.

havior. Kwok and Cunningham [11] described a procedure that uses a series of images to identify the presence of frost flowers as well as their backscatter history. If a Lagrangian element of the ice cover and its associated backscatter histogram can be recorded, any area change and backscatter transients in that Lagrangian element could be identified as that due to thin ice. Given that the older ice (multiyear and thick first-year) has very stable signatures [10] during the winter, the pixel population, which is changing, could be tracked by examining the differences in backscatter histograms of that time series. In view of the laboratory results, if the initial backscatter is close to the lower limit, the ice is thin. In this case, if a strong transient increase in backscatter is observed, it is likely that frost flowers exist on the ice surface. However, we are at a fairly early stage in understanding all processes associated with the growth of frost flowers. Certain conditions seem to be conducive to the formation of this surface layer but are not well documented. As mentioned above, frost flowers seem to be quite prevalent in the winter Arctic. Laboratory measurements help to characterize the signatures variability and provide a link to the physical properties.

C. Flooding and Slush Formation on Thin Ice

Microwave signatures from sea ice are significantly affected by a wet slushy layer on the ice surface. Experimental results show a 1.7-dB increase in reflectivity at normal incidence from -4.4 dB for bare saline ice to -2.7 dB measured immediately after the flooding. This increase corresponds to a large increase in the permittivity of the flooded surface.

The slush layer contains high salinity and has a large relative permittivity with high attenuation of electromagnetic waves. Fig. 7 presents backscatter measurements of bare saline ice and slush covered ice for VV-polarization (top panel of Fig. 7) and HH-polarization (bottom panel of Fig. 7). The ice thickness in these case is 12.6 cm, and the slush layer is approximately 3 mm thick. The results reveal significant decreases in backscatter at both polarizations. The decrease in

σ_{vv} is 4–5 dB, and σ_{hh} is reduced by 4–8 dB at different incidence angles. This may be caused by changes in the thermodynamic phase distribution in the slush layer during the scatterometer measurements. These strong decreases definitively indicate that the wetness in the surface layer is important to sea ice backscatter signatures. A similar situation is that the top surface or the snow cover on sea ice melts when the temperature is above the freezing point. In this case, the wet slushy layer significantly reduces backscatter. Multiyear ice backscatter can decrease significantly due to flooding or the wet surface layer, and its backscatter level becomes lower than that of younger ice, causing a reversal in the backscatter contrast of these ice types. This phenomenon is important during seasonal transition periods, such as onsets of summer melt and fall freeze-up (reverse effect), when transitions in remote-sensing data can be applied to study the spatial and temporal evolutions induced by the seasonal events.

D. Diurnal Effect and Temperature Change

We examined the diurnal changes in the backscatter of thin ice during one of our experiments at the outdoor CRREL GRF. Measurements were taken over a 60-h period, during which the ice sheet grew to a thickness of 10 cm. The effects of the diurnal cycle are shown in Fig. 8. The measurements began during daytime hours when the ice temperature was not too cold due to higher air temperature and insolation. During the night, the temperature decreases as well as the backscatter. In fact, the backscatter closely follows the ice surface temperature variations over both of the diurnal temperature cycles. The experimental results indicate that diurnal effects on backscatter are substantial, there is a positive correlation between backscatter and temperature, and the thermal effect on backscatter is reversible.

In the range of ERS-1 look angles, backscatter measurements of the thin ice sheet show a 3–5-dB increase in the backscatter level during the day, corresponding to the rise in ice surface temperature. It should be noted that the air tem-

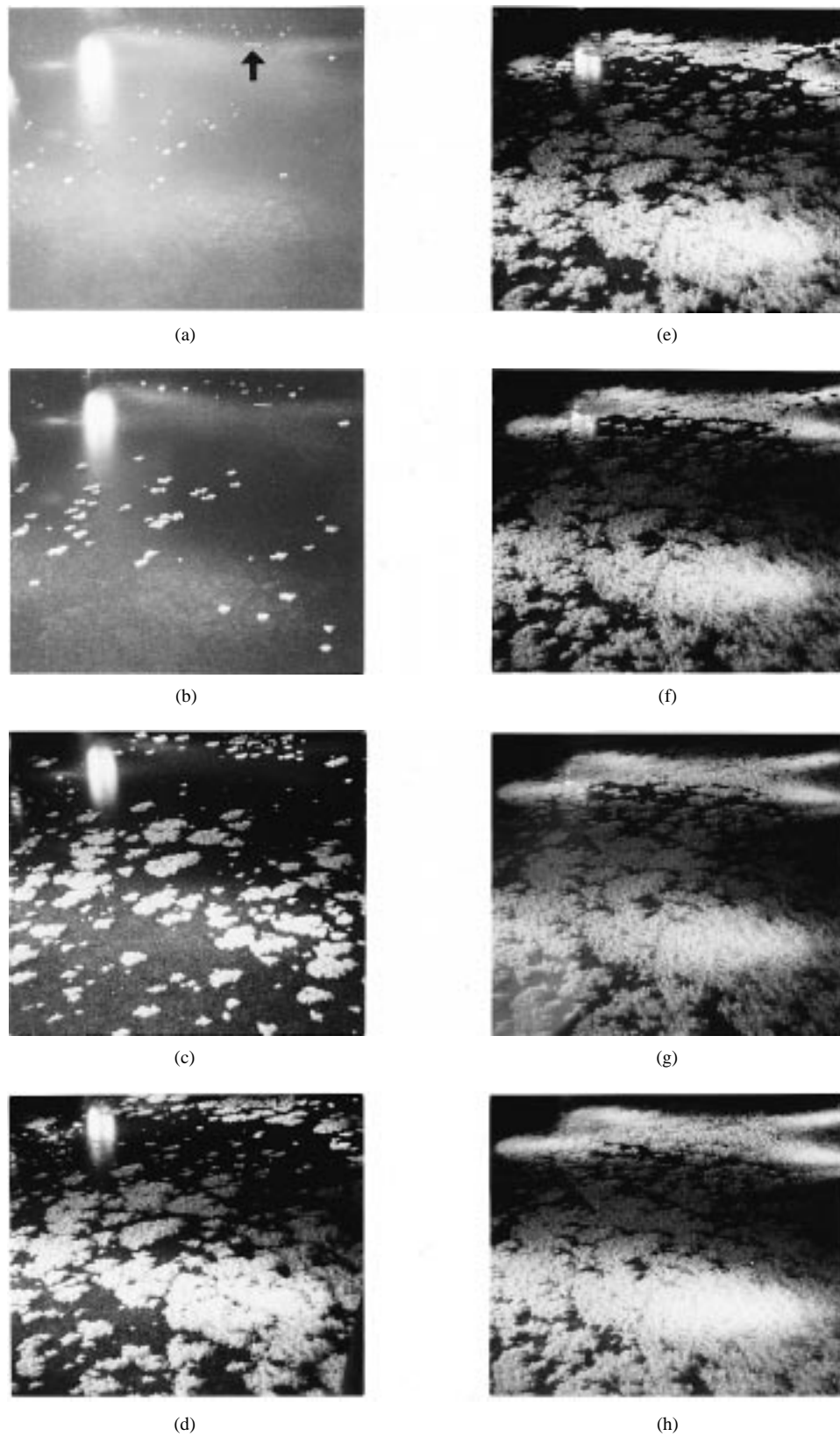


Fig. 5. Growth of frost flowers with increasing areal coverage during a three-day experiment in the CRREL indoor refrigerated facility. White horizontal object indicated by the arrow in panel (a) is a 10-cm ruler for reference.

perature remained below -10° during the entire experiment. The peaks in the backscatter occur during the afternoon. We attribute this increase to the thermal expansion of the brine inclusions and to the increase in sea ice effective permittivity

due to the ice warming. In terms of the absorption of shortwave radiation energy, brine pocket enlargement transforms and consumes energy and becomes a component of the radiative distribution in the heat budget balance [18]. Notice that the

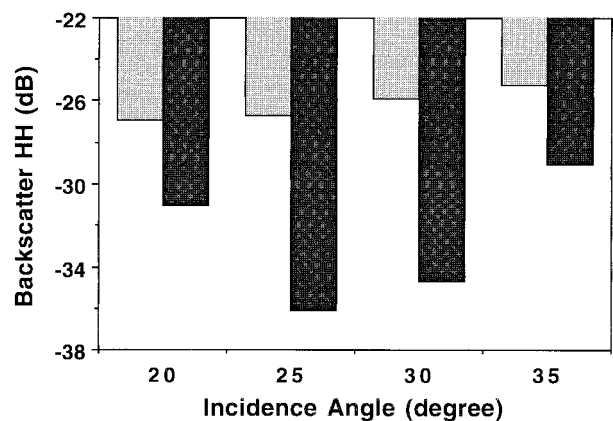
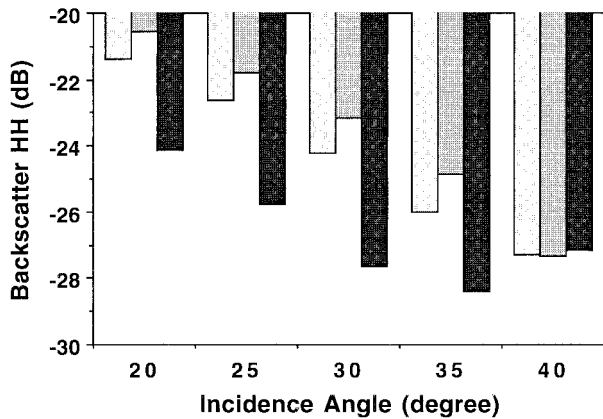
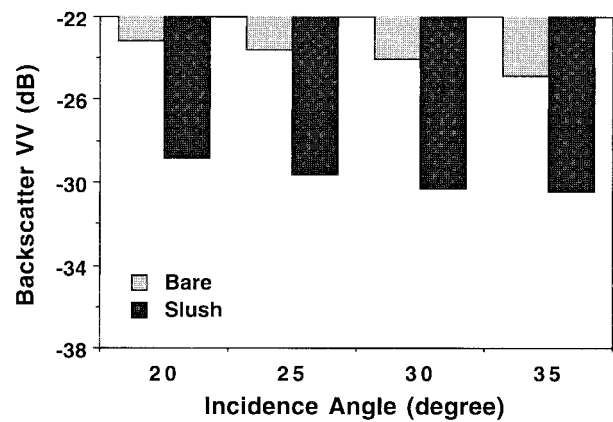
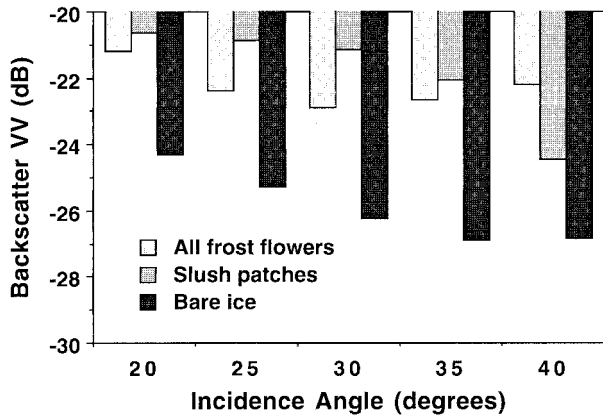


Fig. 6. Effects of frost flowers on backscatter measured with all frost flowers left intact, with flower ice crystals removed leaving slush patches on the ice surface, and then with the slush removed to expose the bare ice surface.

Fig. 7. Effects of a wet or slush layer formation on backscatter measured by comparing backscatter from bare ice and backscatter with slush cover by surface flooding.

diurnal effect is opposite to the effect of surface wetness on thin ice; the backscatter drops in the case of surface wetness.

A similar increase in backscatter due to increasing ice temperature is evident in ERS-1 SAR data from Arctic field experiments. We conducted the experiments in the Canadian Arctic Archipelago to extend laboratory results to natural conditions of the Arctic. We examine bivariate histograms for early consolidation (thick) and late consolidation (thin) ice types in the areas enclosed by rectangles in Fig. 9(a). The results indicate that, when the air temperature increases between two different data sets, there is a detectable increase in backscatter of sea ice with an initial backscattering coefficient below -19 dB, as seen in Fig. 9(b). The bivariate plots for these two thickness classes show that the smooth thick ice responds to the temperature change with an increase in scattering (slope in the tail of the histogram outside of the agreement bounds). Note that backscatter of the thin ice type increases more under this thermodynamic cycle than does the thick ice area.

These effects of diurnal variations or temperature changes are important in the interpretation of sea ice data [24]. Sun synchronous orbits of ERS and RADARSAT along ascending and descending paths of the satellites provide observations of sea ice usually in the late morning and at the end of the day. From field measurements in the Beaufort Sea, [29] indicate that the diurnal cycle of solar radiation in late winter and

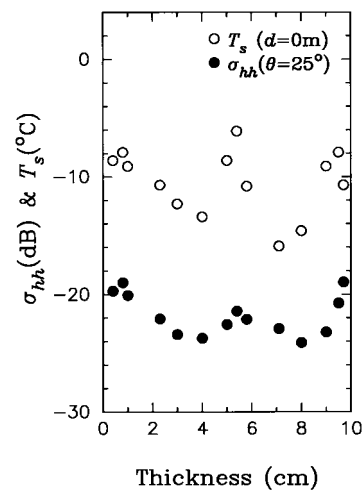


Fig. 8. Variations in backscatter caused by diurnal thermal cycling. The close circles are for backscatter σ_{hh} data at incidence angle $\theta = 25^{\circ}$, and the open circles are for ice surface temperature T_s data.

early spring in the Arctic is similar to that of a midlatitude winter. The diurnal effects on air temperature and backscatter are strong. Therefore, in the late winter, spring, and early fall, variabilities in the backscatter level of thin ice should be interpreted with care; the backscatter variations could be a response to the thermal environment. For consistency in

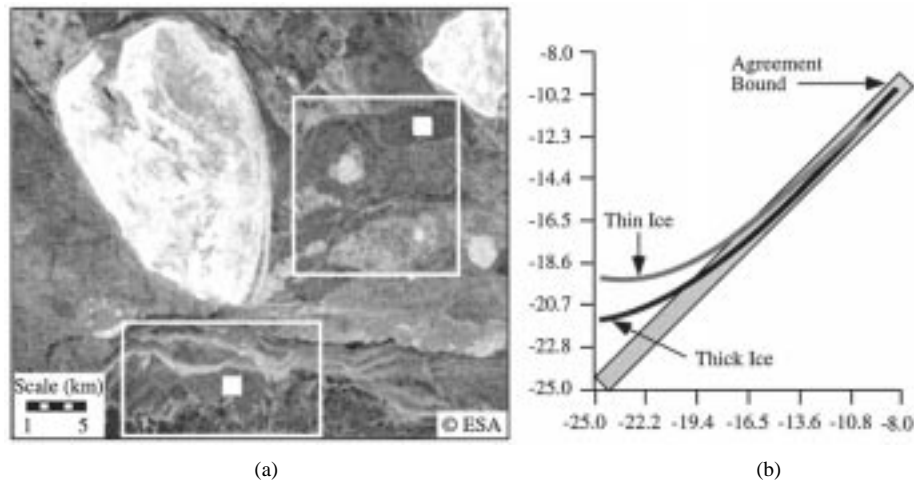


Fig. 9. Field experiments for sea ice in the Canadian Arctic Archipelago: (a) ERS-1 SAR scene of the experimental site, including the subsceen enclosed in the large upper box for an early consolidation surface with thick first-year, multiyear, and rubble ice types, and the subsceen enclosed in the lower box for a late consolidation ice surface with only thin first-year sea ice. (b) Bivariate plots of backscatter in decibels taken at cold temperature for the horizontal axis and at warmer temperature for the vertical axis.

view of the diurnal effects and corresponding temperature changes, data in ascending and descending paths should be separated in the data interpretation of sea ice geophysics. Furthermore, because of the correlation of backscatter with temperature [24], backscatter changes can be exploited to study the corresponding changes in air and ice temperatures.

V. RETRIEVAL OF THIN ICE THICKNESS

Recent analyses of polarimetric SAR observations of sea ice clearly show variations in backscattering signatures with apparent ice thickness, where the apparent thickness is estimated from ancillary data and contextual information in the SAR imagery itself. Although the data sets examined here have yet to include direct *in situ* observations of the actual ice thickness, the evidence for signatures variations of useful magnitude over roughly the range of geophysically important ice thicknesses is compelling.

A. L-Band Polarimetric Observations

Winebrenner *et al.* [34] studied the variations in backscattering signature at 24-cm wavelength. The observed signature variations are not easily explained in terms of conventional modeling of sea ice backscattering, but they have shown that an interaction mechanism directly involving reflection from the ice-water interface and scattering from the air-ice interface can explain the observations. Moreover, this explanation of the signature variations indicates a potential for direct sensing of the thickness of undeformed new ice in the thickness range 0–50 cm using 24-cm wavelength SAR.

The copolar phase of the backscattered signal depends primarily on the range to the target area. The difference between the phases of signals in these two distinct backscattering measurements, however, is characteristic of the scattering process that gives rise to the signal. The copolar phase is typically defined as the (mean) difference in phase between HH- and VV-polarized backscattered signals. Fig. 10 [34] shows copolar ratios and phases at 24-cm wavelength

(L-band), as functions of incidence angles, for several distinct ice types, as observed with the JPL AirSAR in the Beaufort Sea, AK, during 1988. Multiyear ice and (apparently) thick first-year ice display copolar ratios near those expected for scattering from a small-roughness surface bounding effectively infinite thick ice. The corresponding copolar phases cluster around a constant reference value, taken here on theoretical grounds to be 0° . Two different regions of apparently thin, new sea ice, however, display very different signatures. One lead area shows copolar phases approximately 15° less than the reference value (i.e., negative copolar phases), together with copolar ratios intermediate between those expected, and observed, for thick ice and open sea water. A second area from apparently thin first-year ice shows copolar phases 25° above the reference value (positive copolar phases) and copolar ratios slightly below those of thick ice. Although the correlation of HH- and VV-polarized returns for new ice are lower than for thick ice or water, the difference between new ice and other signatures exceeds the uncertainties in their estimation. Moreover, observations of leads in Antarctic pack ice show [33] several examples of leads containing ice of two different ages, evidently due to distinct opening events; the apparently younger ice shows negative copolar phases, whereas the neighboring, apparently older new ice shows positive copolar phases (again, relative to nearby, apparently thick ice). Thus, observations in the two polar regions show new ice types with copolar ratios and phases strongly different from either open water or thick ice. The variation of signatures with apparent thickness suggests a nonmonotonic relation, making it essential to understand the variation physically to infer ice thickness from observations.

An examination of permittivity, permittivity fluctuations, and roughness of new sea ice indicates scattering from the rough air-ice interface to be the dominant source of backscattering from this ice type [35]. However, neither classical rough surface-scattering (assuming an infinite depth of material beneath the rough surface) nor volume-scattering models appropriate to sea ice readily predict nonzero copolar

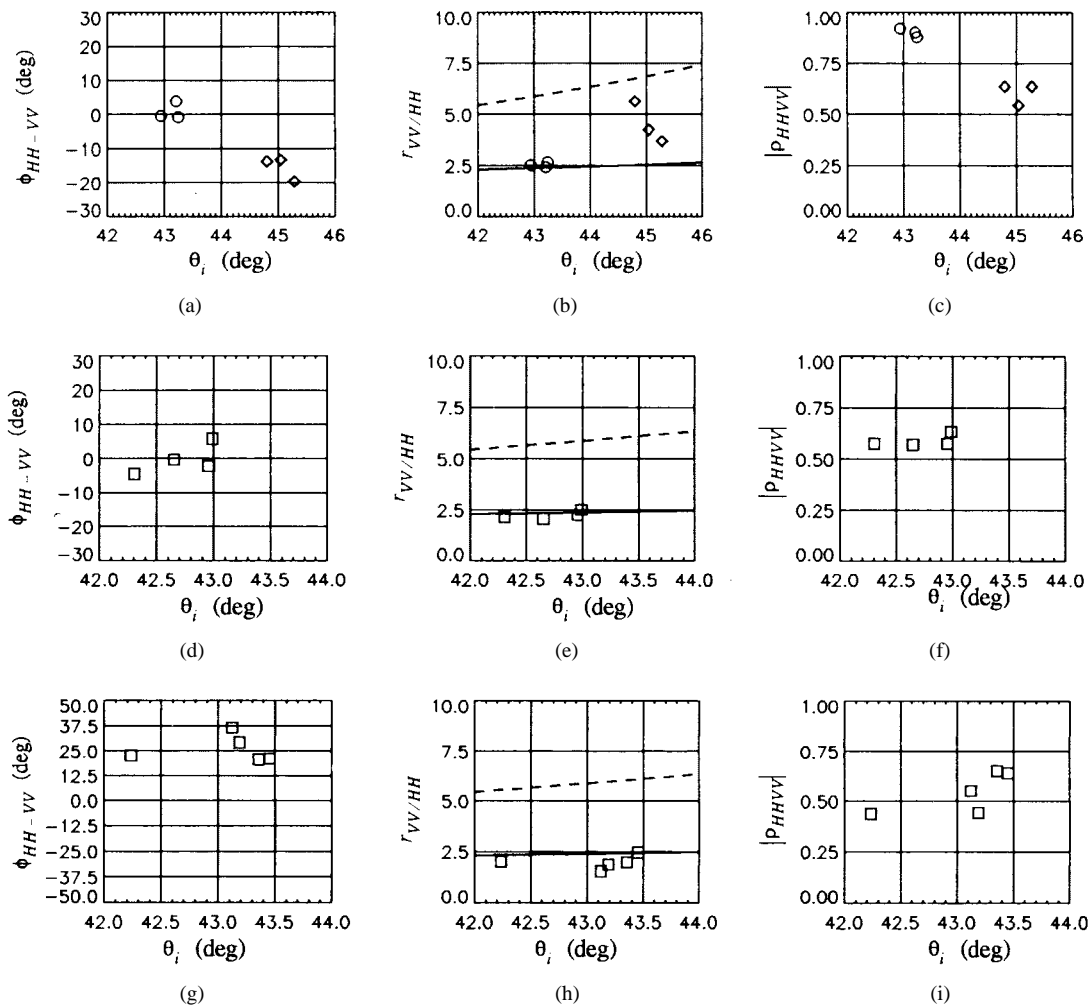


Fig. 10. (a)–(c) Copolar ratios, phases, and correlation magnitudes for multiyear ice and lead ice, and (d)–(f) and (g)–(i) for two distinct groups of first-year ice samples of apparently differing thickness.

phases. This apparent contradiction of observations can be resolved by noting that 24-cm radiation can propagate far enough into new sea ice to be partly reflected back from the ice–water transition zone; partially coherent interference between up- and down-going wave fields in the ice is translated across the rough air–ice interface into the scattered fields in accordance with the boundary conditions at that interface. Variations in this interference with varying thickness lead to varying values of copolar ratios and phases that differ from thick ice or open water values. Random variations in ice thickness over SAR pixels diminishes, but it does not eliminate, this interference. (It is very important, though, that the backscattering observations not be averaged over the large bandwidths common in ground-based radar systems—this does average out all of the interference upon which the signature variation depends.) Quantitative predictions of copolar ratios and phases, as functions of mean ice thickness, show variations of the magnitude observed without tuning parameters in the signature model [34].

Moreover, the predicted trajectory of copolar phase and ratio with increasing thickness is single-valued—thus, time-series observations of polarimetric backscattering, with proper temporal resolution, should be sufficient to estimate new ice

thickness. Note that such an estimation would be based on physics directly involving ice thickness and not on observation of any proxy for thickness, such as ice type or the ice surface condition. Clearly the next, urgently necessary step in developing polarimetric thickness estimation is a quantitative test of our understanding using polarimetric observations (of sufficiently narrow bandwidth) and direct, *in situ* observations of ice thickness. Airborne polarimetric SAR's are excellent platforms for collecting data for pursuing such experimental work.

B. Combined C- and L-Band Polarimetric Observations

Kwok *et al.* [8] demonstrated in one case study that the thickness of thin ice can be retrieved using a neural network trained with results from a scattering model. The results from their polarimetric scattering model seem to explain a large part of the variability of thin ice signature extracted from the JPL polarimetric AirSAR observations. Realistic properties of the sea ice were used in their modeling effort. The details of the scattering model, which accounts for layer effects on both volume- and surface-scattering mechanisms, can be found in [20]. The model was verified with radar measurements of laboratory grown ice [22], [24] and Arctic sea ice [19].

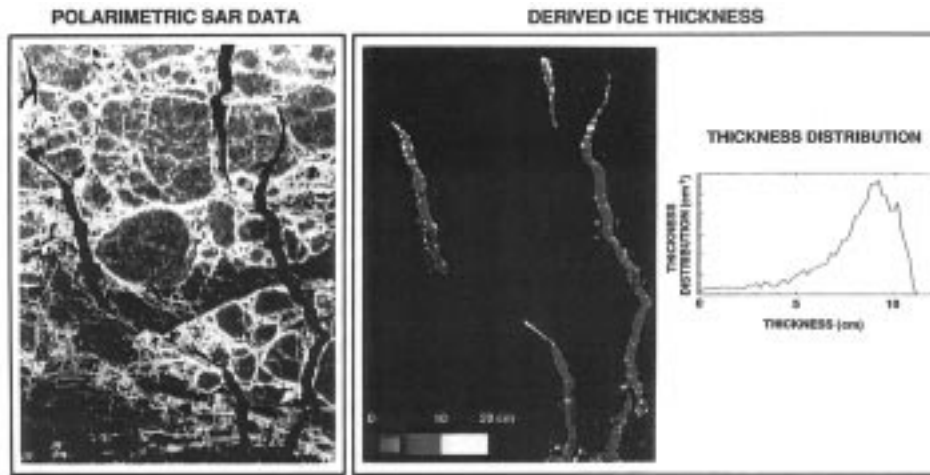


Fig. 11. Retrieval of ice thickness from JPL polarimetric SAR data for young ice in the newly opened leads shown in the sea ice scene on the left panel. Right panel shows the derived thickness and the ice thickness distribution.

This represents an attempt to integrate the knowledge from laboratory measurements, model calculations, and results from field programs to retrieve ice thickness from remote-sensing data sets. In their study, several leads with thin ice were identified using ancillary information and coincident passive microwave observations. The basis of their algorithm was to first mask out potentially confusing thick ice signatures and focus the retrieval process on open leads where there is a higher likelihood of finding thin ice. This is by no means an operational algorithm but an experimental approach. The results for ice thickness derived from JPL C- and L-band polarimetric SAR data are presented in Fig. 11 for thin ice in newly open leads in a Beaufort sea ice scene.

C. Low-Frequency Passive Sensing of Ice Thickness

It is advantageous to combine active and passive microwave data to approach the problem of thickness retrieval for thin sea ice since the mechanisms responsible for active and passive signature of thin sea ice are different. Hence, the information contained in active and passive data regarding ice thickness are complementary. In this respect, we consider brightness temperature measurements with passive radiometers for their sensitivity to the thickness of thin ice.

For passive remote sensing of sea ice, the research undertaken by the University of Massachusetts, Amherst, focused on experimental observations using low-frequency microwave radiometers. The suite of instruments used to observe sea ice at CRREL includes P-, L-, and S-band linearly polarized radiometers, which were mounted on rigs placed alongside the GRF. The primary purpose of the choice of low frequencies to observe the ice is that these frequencies tend to penetrate deep into saline ice so that changes in observed brightness temperature can be correlated with changes in ice thickness during the growth phase. Although P-band will penetrate the deepest, it is doubtful that it will be used for passive microwave remote sensing from space for several reasons, including large antennas, RF interference, and severe interaction with the

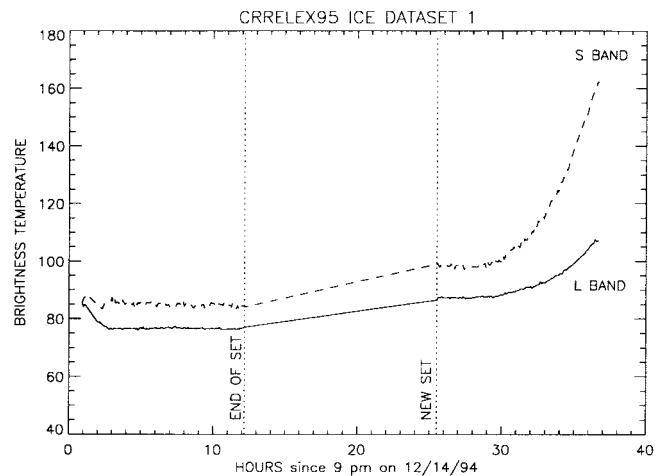


Fig. 12. Brightness temperature measurements at L-band (solid curve) and S-band (dashed curve) frequencies. Data on the left are for smooth open water and on the right for the growth phase of thin ice.

ionosphere. In the followings, we present the case for L- and S-band data.

The attenuation coefficient for electromagnetic waves propagating into a lossy dielectric mixture is given by

$$\alpha = (2\pi f/c)(\sqrt{\epsilon_{\text{eff}}/\epsilon_0})''$$

where f is frequency, c is the speed of light in free space, and $(\sqrt{\epsilon_{\text{eff}}/\epsilon_0})''$ is the imaginary part of the square root of the relative effective permittivity, which measures the loss of electromagnetic wave energy in the material. We note that α becomes smaller as the frequency decreases. Since the penetration depth is the reciprocal of the attenuation coefficient, wave penetration increases with decreasing frequency, which forms the basis of the choice of low-frequency radiometers for sea ice observations. Fig. 12 shows calibrated S-band (dashed line) and L-band brightness temperatures for smooth water (at the left of the figure) and during initial growth of the saline ice sheet. Note that during growth, the S-band brightness temperature increases at a much greater rate as the

ice thickness increases. These observations are consistent with the formula for the attenuation, and is indeed indicative that S- and L-band can be used to detect ice that is several centimeters thick. This capability to sense thin ice types will add value to future satellite remote-sensing systems.

VI. SUMMARY

In this paper, we examined results of microwave measurements of sea ice in the laboratory environment to evaluate potential links to airborne and spaceborne remote-sensing observations. Such connections are essential in the interpretation of sea ice remote-sensing data sets. We have focussed on thin sea ice types because it is important to a number of processes affecting ocean and atmosphere interactions and because it is easily grown in the laboratory conditions.

We summarize scatterometer measurements carried out during a period of three years from 1993 to 1995 at CRREL. Comparisons of physical and structural characteristics of laboratory grown ice with those of natural sea ice show their similarities. We review results of C-band polarimetric scatterometer measurements of thin ice in view of present and future aircraft and satellite SAR's, such as the JPL AirSAR, the Danish EMISAR, the ERS satellites, RADARSAT, and ENVISAT. All of these radars operate at C-band with a variety of polarization capabilities.

From laboratory backscatter data of thin saline ice grown under quiescent conditions at constant temperatures, we suggest lower bounds or limits for remote-sensing data because any perturbation in the natural sea ice growth will increase the backscatter. On the other hand, frost flower experiments indicate strong transient (one–three days) increases in the backscatter of thin ice; this can be used to detect frost flowers grown on new ice using backscatter history in remote-sensing data. A wet, slush layer on thin ice due to surface melt or flooding, as studied in the laboratory, causes significant decreases in backscatter; such effects can be applied to examine backscatter during seasonal transitions with the appearance of liquid water on the ice surface. Backscatter measurements at the outdoor GRF facility reveal strong diurnal effects on backscatter due to thermal cycling of the sea ice volume. This is important for interpretation of satellite data acquired at different times of day (e.g., ascending and descending orbits) because of effects of insolation and temperature cycles.

We also discussed one of the more important problems in sea ice remote sensing—the retrieval of ice thickness from remote-sensing data. We surveyed several potential methods for estimating thickness of thin ice. One is to utilize copolar phase between vertical and horizontal SAR returns at L-band, which relates to the thickness of thin ice (0–50 cm) through a coherent interaction mechanism involving reflections from the ice layer interfaces. The other method is through the use of neural networks to derive ice thickness from a combination of C- and L-band SAR data trained with a sea ice polarimetric layer model. Finally, we considered passive measurements at low frequencies (S- and L-band), which show increases in brightness temperatures as the ice thickens. These are potential thickness retrieval algorithms that could be used with future satellite systems for sea ice remote sensing.

REFERENCES

- [1] D. G. Barber, T. N. Papakyriakou, and E. F. LeDrew, "On the relationship between energy fluxes, dielectric properties, and microwave scattering over snow covered first-year ice during the spring transition period," *J. Geophys. Res.*, vol. 99, no. C11, pp. 22401–22411, 1994.
- [2] S. G. Beaven, S. P. Gogineni, and M. Shanableh, "Radar backscatter signatures of thin sea ice in the central Arctic," *Int. J. Remote Sensing*, vol. 15, no. 5, pp. 1149–1154, 1994.
- [3] D. J. Cavalieri, J. P. Gloersen, and W. J. Campbell, "Determination of sea ice parameters from Nimbus 7 SMMR," *J. Geophys. Res.*, vol. 89, no. D4, pp. 5355–5369, 1984.
- [4] M. R. Drinkwater, R. Hosseinmostafa, and P. Gogineni, "C-band backscatter measurements of winter sea-ice in the Weddell Sea, Antarctica," *Int. J. Remote Sensing*, vol. 16, no. 17, pp. 3365–3389, 1995.
- [5] K. M. Golden, "Bounds on the complex permittivity of sea ice," *J. Geophys. Res.*, vol. 100, no. 13, pp. 699–13, 711, 1995.
- [6] ———, "The interaction of microwaves with sea ice," *Wave Propagation in Complex Media, IMA Volumes in Mathematics and its Applications*, vol. 96, G. Papanicolaou, Ed. Berlin, Germany: Springer-Verlag, 1997, pp. 75–94.
- [7] A. J. Gow and W. B. Tucker, III, *Physical and Dynamic Properties of Sea Ice in the Polar Oceans*, CRREL, Hanover, NH, Mono. 91-1, 1991, p. 46.
- [8] R. Kwok, S. V. Nghiem, S. H. Yueh, and D. D. Huynh, "Retrieval of thin ice thickness from multifrequency polarimetric SAR data," *Remote Sens. Environ.*, vol. 51, no. 3, pp. 461–474, 1995.
- [9] R. Kwok, D. A. Rothrock, H. L. Stern, and G. F. Cunningham, "Determination of ice age using Lagrangian observations of ice motion," *IEEE Trans. Geosci. Remote Sensing*, vol. 33, pp. 392–400, Mar. 1995.
- [10] R. Kwok and G. F. Cunningham, "Backscatter characteristics of the winter sea ice cover in the Beaufort Sea," *J. Geophys. Res.*, vol. 99, no. C4, pp. 7787–7803, 1994a.
- [11] ———, "Use of time series SAR data to resolve ice type ambiguities in newly opened leads," in *Proc. IGARSS'94*, Pasadena, CA, pp. 1024–1026.
- [12] R. Kwok, E. Rignot, B. Holt, and R. G. Onstott, "Identification of sea ice types in spaceborne SAR data," *J. Geophys. Res.*, vol. 97, no. C2, pp. 2391–2402, 1992.
- [13] S. Martin, "A field study of brine drainage and oil entrainment in first-year sea ice," *J. Glaciol.*, vol. 22, pp. 473–502, 1979.
- [14] S. Martin, R. Drucker, and M. Fort, "A laboratory study of frost flower growth on the surface of young sea ice," *J. Geophys. Res.*, vol. 100, pp. 7027–7036, 1995.
- [15] S. Martin, Y. Yu, and R. Drucker, "The effect of frost flower growth at different temperatures on infrared observations of laboratory sea ice," *J. Geophys. Res.*, vol. 101, pp. 12 111–12 125, 1996.
- [16] G. A. Maykut, "Energy exchange over young sea ice in the central Arctic," *J. Geophys. Res.*, vol. 83, no. C7, pp. 3646–3658, 1978.
- [17] ———, "The surface heat and mass balance," in *Geophysics of Sea Ice*, Series B: Physics, vol. 146, N. Untersteiner, Ed. New York: Plenum, 1986, p. 423.
- [18] R. E. Moritz and D. K. Perovich, Eds., *SHEBA, A Research Program on the Surface Heat Budget of the Arctic Ocean*, Science Plan, Univ. Washington, Seattle, Rep. 5, 1996, p. 64.
- [19] S. V. Nghiem, R. Kwok, S. H. Yueh, and M. R. Drinkwater, "Polarimetric signatures of sea ice, 2, Experimental observations," *J. Geophys. Res.*, vol. 100, no. C7, pp. 13 681–13 698, 1995a.
- [20] ———, "Polarimetric signatures of sea ice, 1, Theoretical model," *J. Geophys. Res.*, vol. 100, no. C7, pp. 13 665–13 679, 1995b.
- [21] S. V. Nghiem, R. Kwok, J. A. Kong, R. T. Shin, S. A. Arcone, and A. J. Gow, "An electrothermodynamic model with distributed properties for effective permittivities of sea ice," *Radio Sci.*, vol. 31, no. 2, pp. 297–311, 1996.
- [22] S. V. Nghiem, R. Kwok, S. H. Yueh, A. J. Gow, D. K. Perovich, J. A. Kong, and C.-C. Hsu, "Evolution in polarimetric signatures of thin saline ice under constant growth," *Radio Sci.*, vol. 32, no. 1, pp. 127–151, 1997a.
- [23] S. V. Nghiem, S. Martin, D. K. Perovich, R. Kwok, R. Drucker, and A. J. Gow, "A laboratory study of the effects of frost flowers on C-band radar backscatter from sea ice," *J. Geophys. Res.*, vol. 102, no. C2, pp. 3357–3370, 1997b.
- [24] S. V. Nghiem, R. Kwok, S. H. Yueh, D. K. Perovich, A. J. Gow, C.-C. Hsu, K. H. Ding, J. A. Kong, and T. C. Grenfell, "Diurnal thermal cycling effects on microwave signatures of thin sea ice," *IEEE Trans. Geosci. Remote Sensing*, vol. 36, pp. 111–124, Jan. 1998.
- [25] R. G. Onstott, "SAR and scatterometer signatures of sea ice," in

- Microwave Remote Sensing of Sea Ice*, F. D. Carsey, Ed. Washington, DC: Amer. Geophys. Union, Geophys. Mono. 68, 1992, pp. 73-104.
- [26] D. K. Perovich and J. A. Richter-Menge, "Surface characteristics of lead ice," *J. Geophys. Res.*, vol. 99, no. C8, pp. 16 341-16 350, 1994.
- [27] D. K. Perovich and A. J. Gow, "A quantitative description of sea ice inclusion," *J. Geophys. Res.*, vol. 101, pp. 18 327-18 343, 1996.
- [28] E. Rignot and M. Drinkwater, "Winter sea ice mapping from multi-parameter synthetic aperture radar," *J. Glaciol.*, vol. 40, no. 134, pp. 31-45, 1994.
- [29] D. Ruffieux, P. O. G. Persson, C. W. Fairall, and D. E. Wolfe, "Ice pack and lead surface energy budgets during LEADDEX 1992," *J. Geophys. Res.*, vol. 100, no. C3, pp. 4953-4612, 1995.
- [30] R. Sawicz, and K. M. Golden, "Bounds on the complex permittivity of matrix-particle composites," *J. Appl. Phys.*, vol. 78, pp. 7240-7246, 1995.
- [31] L. M. H. Ulander, A. Carlström, and J. Askne, "Effect of frost flowers, rough saline snow and slush on the ERS-1 backscatter of thin Arctic sea-ice," *Int. J. Remote Sensing*, vol. 16, no. 17, pp. 3287-3305, 1995.
- [32] W. F. Weeks and S. F. Ackley, *The Growth, Structure and Properties of Sea Ice*, CRREL, Hanover, NH, Mono. 82-1, 1982, p. 130.
- [33] D. P. Winebrenner, "Polarimetric backscattering at 23 cm wavelength from Antarctic lead ice and estimation of ice thickness," in *Proc. Int. Geosci. Remote Sens. Symp.*, 1996.
- [34] D. P. Winebrenner, L. D. Farmer, and I. R. Joughin, "On the response of polarimetric synthetic aperture radar signatures at 24-cm wavelength to sea ice thickness in Arctic leads," *Radio Sci.*, vol. 30, no. 2, pp. 373-402, 1995.
- [35] D. P. Winebrenner, J. Bredow, A. K. Fung, M. R. Drinkwater, S. V. Nghiem, A. J. Gow, D. K. Perovich, T. C. Grenfell, H. C. Han, J. A. Kong, J. K. Lee, S. Mudaliar, R. G. Onstott, L. Tsang, and R. D. West, "Microwave sea ice signature modeling," in *Microwave Remote Sensing of Sea Ice*, F. Carsey, Ed. Washington, DC: Amer. Geophys. Union, Geophys. Mono. 68, 1992.
- S. Martin**, photograph and biography not available at the time of publication.
- D. P. Winebrenner** (S'79-M'79-SM'90), photograph and biography not available at the time of publication.
- Anthony J. Gow**, for a photograph and biography, see p. 124 of the January 1998 issue of this TRANSACTIONS.
- Donald K. Perovich**, for a photograph and biography, see p. 124 of the January 1998 issue of this TRANSACTIONS.
- C. T. Swift** (M'67-SM'69-F'83), photograph and biography not available at the time of publication.
- David G. Barber**, for a photograph and biography, see p. 50 of the January 1998 issue of this TRANSACTIONS.
- Ronald Kwok** (S'82-M'84), for a photograph and biography, see p. 37 of the January 1998 issue of this TRANSACTIONS.
- K. M. Golden**, photograph and biography not available at the time of publication.
- Son V. Nghiem** (M'86), for a photograph and biography, see p. 123 of the January 1998 issue of this TRANSACTIONS.
- E. J. Knapp**, photograph and biography not available at the time of publication.